

Coulomb dissociation of the deformed halo nucleus ^{31}Ne

Y. Urata,¹ K. Hagino,¹ and H. Sagawa²

¹ Department of Physics, Tohoku University, Sendai, 980-8578, Japan

² Center for Mathematics and Physics, University of Aizu, Aizu-Wakamatsu, Fukushima 965-8560, Japan

The recently observed large cross sections for the Coulomb dissociation of ^{31}Ne nucleus indicate that this nucleus takes a halo structure in the ground state. We analyse these experimental data using the particle-rotor model, that takes into account the rotational excitation of the core nucleus ^{30}Ne . We show that the experimental data can be well reproduced when the quadrupole deformation parameter of ^{30}Ne is around $\beta_2 = 0.2 \sim 0.3$, at which the ground state takes the spin and parity of $I^\pi=3/2^-$. This state corresponds to the Nilsson level [330 1/2] in the adiabatic limit of the particle-rotor model. On the other hand, the state corresponding to the Nilsson level [321 3/2] with $\beta_2 \sim 0.55$ can be excluded when the finite excitation energy of the core is taken into account, even though this configuration is a candidate for the ground state of ^{31}Ne in the Nilsson model analysis. We discuss briefly also a possibility of the $I^\pi=1/2^+$ configuration with $\beta_2 \sim 1$ and $\beta_2 \sim -0.4$.

PACS numbers: 21.10.Gv, 21.60.-n, 25.60.Gc, 27.30.+t

A halo structure with an extended density distribution is one of the characteristic features of weakly bound neutron-rich nuclei. It was first recognized in ^{11}Li , showing an abnormally large interaction cross section [1]. Other examples include ^{11}Be [2, 3] and ^{19}C [4], both of which are typical one-neutron halo nuclei. The root-mean-square radius diverges for s and p waves as the single-particle energy approaches to zero [5], and the halo structure has been ascribed to an occupation of an $l = 0$ or $l = 1$ orbit by the valence neutron [6].

The halo structure induces a large concentration of the electric dipole (E1) strength in the low-excitation energy region, that is, a soft E1 excitation [4, 7, 8]. Recently, the Coulomb breakup cross sections for ^{31}Ne were measured by Nakamura *et al.* [9], indicating a soft E1 excitation in the ^{31}Ne nucleus. Notice that a naive spherical shell model leads to the $1f_{7/2}$ configuration for the valence neutron of ^{31}Ne . In order to generate the halo structure within the mean-field picture, the valence neutron therefore needs to move in a deformed mean-field potential in which the s or p wave component in a weakly-bound single-particle wave function makes a dominant contribution [10–12]. Based on this idea, Hamamoto has carried out Nilsson model calculations with a deformed Woods-Saxon potential, and argued that the large Coulomb dissociation cross sections of ^{31}Ne can be understood if the valence neutron occupies [330 1/2], [321 3/2], or [200 1/2] Nilsson levels [13] leading to $I^\pi = 3/2^-$ ([330 1/2] and [321 3/2] configurations) or $1/2^+$ ([200 1/2] configuration) for the spin and parity of the ground state of ^{31}Ne . We mention that the ground state with $I^\pi = 3/2^-$ is found also with shell model calculations [9, 14] as well as with a microscopic cluster model calculation [15].

In order to describe odd-mass deformed nuclei, especially nuclei with small deformation as well as transitional nuclei, the particle-rotor model (PRM) has been applied with great success [16–18]. It was also applied successfully to a halo nucleus ^{11}Be [19, 20] and neutron-rich Carbon isotopes $^{15,17,19}\text{C}$ [21]. In ^{30}Ne , the candidates for the first excited 2^+ and 4^+ states have been

identified experimentally at excitation energies of 0.801 MeV and 2.24 MeV, respectively [22, 23]. The energy ratio $E_{4^+}/E_{2^+}=2.80$ suggests this nucleus to be a transitional one in comparison with the ratio 3.33 for well-deformed nuclei. Although the experimental uncertainty is still large, an extremely small neutron separation energy $S_n=0.29\pm1.64$ MeV [24] suggests a halo structure of ^{31}Ne . Because of these reasons, in this paper we assume a deformed ^{30}Ne core and adopt the particle-rotor model to study the ground state and the excited state properties of ^{31}Ne .

The Nilsson model adopted in Ref. [13] to analyze the ground state configuration of ^{31}Ne corresponds to a strong coupling limit of the particle-rotor model. That is, the non-adiabatic effect due to the rotational states of the deformed core was neglected in the analysis. In general, in deformed nuclei with mass $A \lesssim 40$, the rotational energy is not small, and the non-adiabatic effect may play a role in discussing physical observables such as electric dipole (E1) transitions. While the non-adiabatic effect may be estimated perturbatively in the Nilsson model, especially to determine the spin and parity of the nucleus in the laboratory frame [16, 17], it is not obvious whether the perturbation works for the particular case of ^{31}Ne nucleus. In this respect, it is highly desirable to disentangle how much the non-adiabatic effect appears in the assignment of the spin-parity of the ground state and also in the E1 transitions of ^{31}Ne .

The aim of this paper is thus to study the ^{31}Ne nucleus by solving the particle-rotor model Hamiltonian without resorting to the adiabatic approximation and discuss the E1 excitation and the Coulomb breakup cross sections. In order to describe the structure of the ^{31}Ne nucleus, we assume that the core nucleus ^{30}Ne is statically deformed with a quadrupole deformation parameter β_2 and the motion of the valence neutron is coupled to the rotational motion of the core nucleus. Assuming the axially symmetric shape of the core nucleus, we consider the fol-

lowing Hamiltonian for the $^{30}\text{Ne}+n$ system:

$$H = -\frac{\hbar^2}{2\mu}\nabla^2 + V(\mathbf{r}, \hat{\mathbf{r}}_c) + H_{\text{rot}}, \quad (1)$$

where $\mu = m_N A_c / (A_c + 1)$ is the reduced mass of the valence neutron with $A_c=30$ and m_N being the mass number of the core nucleus and the nucleon mass, respectively. H_{rot} is the rotational Hamiltonian for the core nucleus given by $H_{\text{rot}} = \mathbf{I}_c^2 \hbar^2 / 2\mathcal{J}$, where \mathbf{I}_c is the spin of the core nucleus and \mathcal{J} is the moment of inertia. V is the single-particle potential for the valence neutron interacting with the deformed core. \mathbf{r} and $\hat{\mathbf{r}}_c$ are the coordinate of the valence neutron and the direction of the symmetry axis of the core nucleus in the laboratory frame, respectively. For the single-particle potential V , we use a deformed Woods-Saxon potential,

$$V(\mathbf{r}, \hat{\mathbf{r}}_c) = -V_{\text{WS}} \left(1 - F_{\text{ls}} r_0^2 (\mathbf{l} \cdot \mathbf{s}) \frac{1}{r} \frac{d}{dr} \right) f(r) \\ + V_{\text{WS}} R_0 \beta_2 \frac{df(r)}{dr} Y_{20}(\hat{\mathbf{r}}_{\text{cn}}), \quad (2)$$

$$\equiv V_0(r) + V_2(r) Y_{20}(\hat{\mathbf{r}}_{\text{cn}}), \quad (3)$$

where $\hat{\mathbf{r}}_{\text{cn}}$ is the angle between $\hat{\mathbf{r}}$ and $\hat{\mathbf{r}}_c$, and $f(r)$ is given by

$$f(r) = 1 / [1 + \exp((r - R_0)/a)], \quad (4)$$

with $R_0 = r_0 A_c^{1/3}$. Here, for simplicity, we have expanded the deformed Woods-Saxon potential up to the linear order of β_2 . We have checked that this approximation works for the range of deformation parameter considered in this paper, by comparing our results for the Nilsson model with the numerical results obtained with the code `WSBETA`[25].

In principle, the eigenfunctions of the Hamiltonian (1) can be obtained by solving the coupled-channels equations in the coordinate space both for the bound and the scattering states [19, 21, 26]. A continuum B(E1) distribution can then be constructed with those scattering wave functions. However, since the experimental data are so far available only in the form of inclusive cross sections, we will not discuss the detailed structure of the strength distribution here but leave it for future publications. It is sufficient for our purpose to expand the wave function on some basis and compute a discrete strength distribution. We do this with the eigenfunctions of the spherical part of the potential V ,

$$\left[-\frac{\hbar^2}{2\mu}\nabla^2 + V_0(r) - \epsilon_{njl} \right] R_{njl}(r) \mathcal{Y}_{jlm}(\hat{\mathbf{r}}) = 0, \quad (5)$$

where $R_{njl}(r)$ is the radial wave function and $\mathcal{Y}_{jlm}(\hat{\mathbf{r}})$ is the spin-angular function. The continuum spectrum can be discretized within a large box. Together with the rotational wave function $\phi_{I_c M_c}(\hat{\mathbf{r}}_c)$, the total wave function for the $n+^{30}\text{Ne}$ system is expanded as,

$$\Psi_{IM}(\mathbf{r}, \hat{\mathbf{r}}_c) = \sum_{njl} \sum_{I_c} \alpha_{njlI_c}^{(I)} R_{njl}(r) [\mathcal{Y}_{jl}(\hat{\mathbf{r}}) \phi_{I_c}(\hat{\mathbf{r}}_c)]^{(IM)}, \quad (6)$$

where I is the spin of ^{31}Ne and M is its z -component. The expansion coefficients $\alpha_{njlI_c}^{(I)}$ as well as the corresponding eigenenergy for the ^{31}Ne nucleus are obtained by numerically diagonalizing the Hamiltonian H .

In order to identify the ground state configuration, we first solve the Hamiltonian by setting $H_{\text{rot}} = 0$ in Eq. (1). In this case, the K quantum number, that is, the projection of the total angular momentum onto the z -axis in the body-fixed frame, is conserved, and several states with different I , having the same value of K , are degenerate in energy when the maximum value of I_c included in the calculation is sufficiently large. As has been shown in Ref. [26], the wave function in this limit is related to the wave function in the Nilsson model, ϕ_{jIK} , as,

$$\sum_n \alpha_{njlI_c}^{(I)} R_{njl}(r) = A_{jI_c}^{IK} \phi_{jIK}(r), \quad (7)$$

where

$$A_{jI_c}^{IK} = \sqrt{\frac{2I_c + 1}{2I + 1}} \cdot \sqrt{2} \langle jKI_c 0 | IK \rangle, \quad (8)$$

and ϕ_{jIK} satisfies [27]

$$\left[-\frac{\hbar^2}{2\mu}\nabla^2 + V(\mathbf{r}, \hat{\mathbf{r}}_c = 0) - \epsilon_K \right] \left(\sum_{j,l} \phi_{jIK}(r) \mathcal{Y}_{jIK}(\hat{\mathbf{r}}) \right) = 0. \quad (9)$$

One can regard Eq. (7) as a transformation of the Nilsson wave function from the body-fixed frame to the laboratory frame, where the angular momentum is conserved. Notice that

$$\sum_{I_c} \sum_n |\alpha_{njlI_c}^{(I)}|^2 = \int r^2 dr \phi_{jIK}(r)^2 = P_{jl}^{(\text{Nil})}, \quad (10)$$

is the probability of each (j, l) component in the Nilsson wave function and is independent of I when $H_{\text{rot}} = 0$.

In this limit, we therefore obtain a collection of Nilsson levels. As usual, we put two neutrons to each Nilsson orbit from the bottom of the potential well, and seek the Nilsson orbit which is occupied by the last unpaired neutron. We then gradually increase the value of the 2^+ energy of the core nucleus up to the physical value, $E_{2^+} = 0.801$ MeV, and monitor how the Nilsson orbit for the valence neutron evolves. For a finite value of E_{2^+} , the K quantum number is not conserved any more due to the Coriolis coupling, and the degeneracy with respect to I is resolved. We select the lowest energy state among several I at $E_{2^+} = 0.801$ MeV as the ground state of ^{31}Ne . In this way, we take into account the Pauli principle between the valence neutron and the neutrons in the core nucleus.

Table I shows the probability of each component, $P_{jI_c} = \sum_n |\alpha_{njlI_c}^{(I)}|^2$, in the wave function for $\beta_2 = 0.1, 0.2$ and 0.55 with two different values of the ground state energy of ^{31}Ne . The ground state energy obtained by diagonalizing the Hamiltonian H is measured from the threshold of $n+^{30}\text{Ne}$, and thus it is equivalent (except

TABLE I: The probability of the component $[I_c \otimes (jl)]$ in deformed wave functions of ^{31}Ne , where I_c is the spin of the rotational state of the core nucleus ^{30}Ne and (jl) is the angular momentum between the valence neutron and the core nucleus. These are obtained with the particle-rotor model (PRM), where the results with vanishing rotational energy, $E_{2+}=0$, correspond to the Nilsson model calculations. The states with $\beta_2=0.1$ and 0.2 correspond to the Nilsson orbit $[330\ 1/2]$ while the state with $\beta_2=0.55$ corresponds to the Nilsson orbit $[321\ 3/2]$. The K^π quantum number is therefore $K^\pi=1/2^-$ and $K^\pi=3/2^-$, respectively. The spin of ^{31}Ne in the laboratory frame is $I^\pi = 3/2^-$ for $\beta_2=0.2$ and 0.55 while it is $7/2^-$ for $\beta_2=0.1$. Two different values of the one neutron separation energy S_n of the ^{31}Ne nucleus are compared. For the case of $E_{2+} = 0$, we also list the total $p_{3/2}$ and $f_{7/2}$ probabilities defined as $P_{jl} \equiv \sum_{I_c} P_{jlI_c}$.

	$[0^+ \otimes p_{3/2}]$	$[2^+ \otimes p_{3/2}]$	(total $p_{3/2}$)	$[2^+ \otimes p_{1/2}]$	$[0^+ \otimes f_{7/2}]$	$[2^+ \otimes f_{7/2}]$	$[4^+ \otimes f_{7/2}]$	(total $f_{7/2}$)
$S_n=0.3\text{ MeV}$								
$\beta_2=0.1, E_{2+} = 0$ (Nilsson)	0%	19.5%	30.3%	0%	17.2 %	20.5%	18.1 %	68.8%
$E_{2+} = 0.801\text{ MeV}$ (PRM)	0%	6.5%	-	0 %	75.2%	17.5 %	0.5 %	-
$\beta_2=0.2, E_{2+} = 0$ (Nilsson)	22.2%	22.2%	44.4%	2.9%	0%	33.5 %	18.6 %	52.1%
$E_{2+} = 0.801\text{ MeV}$ (PRM)	44.9%	8.4%	-	2.0%	0%	42.7 %	1.5 %	-
$\beta_2=0.55, E_{2+} = 0$ (Nilsson)	11.4%	11.5%	22.9%	0%	0%	25.5 %	45.9 %	71.4 %
$E_{2+} = 0.801\text{ MeV}$ (PRM)	1.9%	29.7%	-	4.4%	0%	23.0 %	35.5 %	-
$S_n=0.1\text{ MeV}$								
$\beta_2=0.1, E_{2+} = 0$ (Nilsson)	0%	26.7%	41.5%	0%	14.3%	17.0%	15.0%	57.1%
$E_{2+} = 0.801\text{ MeV}$ (PRM)	0%	7.2%	-	0%	74.8%	17.1%	0.5%	-
$\beta_2=0.2, E_{2+} = 0$ (Nilsson)	26.5%	26.5%	53.1%	3.8%	0%	27.4 %	15.2 %	42.6%
$E_{2+} = 0.801\text{ MeV}$ (PRM)	53.4%	8.3%	-	2.1%	0%	34.6 %	1.2 %	-
$\beta_2=0.55, E_{2+} = 0$ (Nilsson)	12.9%	12.9%	25.7%	0%	0%	24.6 %	44.2 %	68.8 %
$E_{2+} = 0.801\text{ MeV}$ (PRM)	1.8%	30.9%	-	4.9%	0%	23.6 %	33.5 %	-

for the negative sign) to the one-neutron separation energy, S_n (it should not be confused with the energy ϵ_{njl} in Eq. (5)). Following Ref. [13], we use $r_0=1.27\text{ fm}$, $a=0.67\text{ fm}$, and $F_{\text{ls}}=0.44$ for the parameters of the Woods-Saxon potential, (4). V_{WS} is adjusted to reproduce a given value of S_n . We use $R_{\text{box}}=60\text{ fm}$ for the size of the box to discretize the continuum spectrum, and include the single-particle orbits (5) up to $\epsilon = 90\text{ MeV}$ and $l_{\text{max}}=10$. For the spin of the rotational states of the core nucleus, we include up to $I_c = 8$. In the case of vanishing rotational energy, the states with $\beta_2=0.1$ and 0.2 correspond to the Nilsson orbit $[330\ 1/2]$ ($K^\pi = 1/2^-$) while the state with $\beta_2=0.55$ corresponds to the Nilsson orbit $[321\ 3/2]$ ($K^\pi = 3/2^-$). See *e.g.*, Fig. 2 in Ref. [13] for the Nilsson diagram. The spin of ^{31}Ne in the laboratory frame is $I^\pi = 3/2^-$ for $\beta_2=0.2$ and 0.55 , while it is $I^\pi = 7/2^-$ for $\beta_2=0.1$.

In the adiabatic limit (that is, the Nilsson model), for a given j and l , the contribution of each component of $[I_c \otimes (jl)]$ with different value of I_c to the E1 excitation is similar to each other since the radial dependence of the wave function is identical (see Eq. (7)). Therefore, the relevant quantity in this limit is the total probability for each j and l given by Eq. (10). On the other hand, in the case of finite rotational energy (*i.e.*, the non-adiabatic coupling), the radial dependence of the wave function largely depends on I_c . The wave function is spatially most extended for the component

which couples to $I_c = 0$, as the absolute value of the diagonal energy $E - E_{\text{rot}}$ is the smallest (that is, most weakly bound). Therefore, the relevant quantity in this case to the E1 excitation is the probability of the $I_c = 0$ component. In the case of $\beta_2 = 0.2$, the probability of $[0^+ \otimes p_{3/2}]$ increases considerably as the rotational energy increases from zero to 0.801 MeV , and the probability at $E_{2+} = 0.801\text{ MeV}$ is similar to the total $p_{3/2}$ probability in the adiabatic limit. As the separation energy decreases from $S_n=0.3\text{ MeV}$ to $S_n=0.1\text{ MeV}$, the total p -wave probability increases in the adiabatic limit [10–13], and correspondingly the probability of $[0^+ \otimes p_{3/2}]$ also increases in the non-adiabatic case. In contrast, in the case of $\beta_c = 0.55$, the probability of $[0^+ \otimes p_{3/2}]$ decreases considerably as the rotational energy increases. The probability remains small even if the separation energy decreases from $S_n=0.3\text{ MeV}$ to $S_n=0.1\text{ MeV}$. We have confirmed that this is the case even when the separation energy is as small as $S_n = 0.01\text{ MeV}$. We thus expect that the dissociation cross section decreases significantly for this configuration due to the non-adiabatic effect. In the case of $\beta_2 = 0.1$, the $[0^+ \otimes f_{7/2}]$ component increases significantly for the non-adiabatic coupling. Since the f -wave does not form a halo structure, the E1 excitation probability will decrease considerably if the rotational energy is taken into account. As the separation energy decreases, the p -wave component will increase in the Nilsson wave function. However, the non-adiabatic effect always quenches

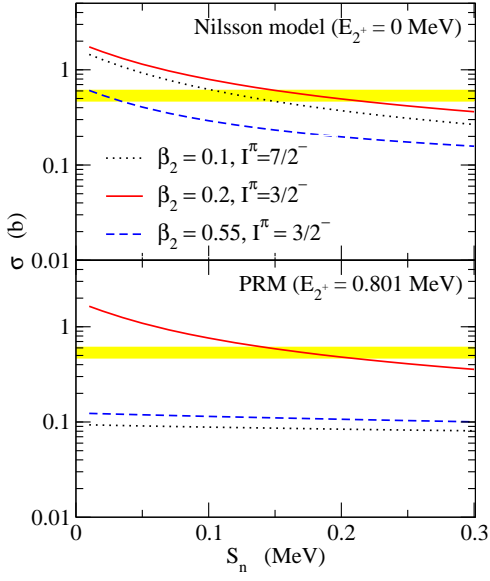


FIG. 1: (Color online) The Coulomb dissociation cross sections of the ^{31}Ne nucleus as a function of the one-neutron separation energy S_n . The upper panel shows the results of the Nilsson model calculations, while the lower panel shows the results with a finite rotational energy of the core nucleus. The dotted, the solid, and the dashed lines denote the results with $\beta_2 = 0.1, 0.2$, and 0.55 , respectively, where the spin and the parity of the ground state is $7/2^-$, $3/2^-$, and $3/2^-$, respectively. The shaded region indicates the experimental data [9].

the p -wave component in this weak coupling regime, and one could not expect large Coulomb dissociation cross sections with this configuration.

Let us now numerically compute the Coulomb dissociation cross sections and confirm the above behaviors discussed in the previous paragraph. To this end, we first compute the E1 strength,

$$B(E1; i \rightarrow f) = \frac{1}{2I_i + 1} \left| \langle \Psi_f | \hat{D} | \Psi_i \rangle \right|^2, \quad (11)$$

where the initial and final wave functions, Ψ_i and Ψ_f , have the same form as in Eq. (6), and the dipole operator \hat{D}_μ is given by $\hat{D}_\mu = -[Z_c e / (A_c + 1)] \cdot r Y_{1\mu}(\hat{r})$. The Coulomb dissociation cross sections can be obtained by multiplying the E1 virtual photon number, N_{E1} , to the $B(E1)$ strength [28–30]. Summing all the final states, the inclusive Coulomb breakup cross section reads,

$$\sigma = \sum_f \frac{16\pi^3}{9\hbar c} \cdot N_{E1}(E_f - E_i) \cdot B(E1; i \rightarrow f). \quad (12)$$

Since we compare our results with the experimental data for the dissociation cross sections, we restrict the summation in Eq. (12) only to those states above the threshold.

Figure 1 shows the Coulomb dissociation cross sections for the three configurations listed in Table I. Since the empirical separation energy S_n has a large uncertainty,

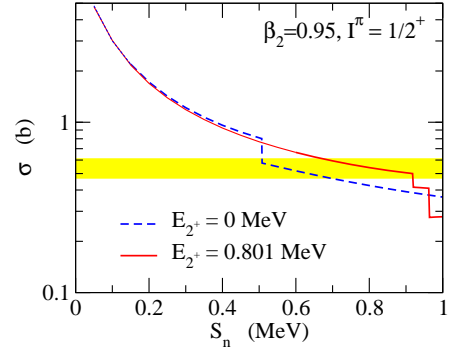


FIG. 2: (Color online) The Coulomb dissociation cross sections of the ^{31}Ne nucleus as a function of the one-neutron separation energy S_n at $\beta_2 = 0.95$. The corresponding Nilsson orbit is $[200\ 1/2]$ ($K^\pi = 1/2^+$), and the spin-parity of the ground state is $I^\pi = 1/2^+$. The dashed and the solid lines denote the results in the adiabatic limit and in the non-adiabatic case, respectively.

we plot the calculated cross sections as a function of S_n . The upper panel shows the results obtained in the adiabatic limit, while the lower panel shows the results with the finite rotational energy. The dotted, solid, and the dashed lines are obtained with $\beta_2 = 0.1, 0.2$, and 0.55 , respectively. The shaded region indicates the experimental data [9]. One can clearly see in the lower panel of Fig. 1 that the experimental data can be well reproduced with $\beta_2 = 0.2$ if the separation energy S_n is around 0.17 MeV. The results remain almost the same even if we vary the deformation parameter in the range of $0.17 \lesssim \beta_2 \lesssim 0.33$. On the other hand, the cross sections obtained with $\beta_2 = 0.1$ and 0.55 appear too small to account for the experimental data. These configurations may yield a reasonable reproduction of the experimental data in the adiabatic limit because of the p -wave dominance in the wave function, but it is simply an artifact of the adiabatic approximation. The non-adiabatic effect eliminates the possibility of these configurations to be the ground state of ^{31}Ne . All of these behaviors agree with the expectations.

Besides the configuration with $\beta_2 \sim 0.2$, there may be other possibilities for the ground state configuration of ^{31}Ne . It was argued in Ref. [13] that the $I^\pi = 1/2^+$ configuration originated from the $[200\ 1/2]$ Nilsson orbit ($K^\pi = 1/2^+$) cannot be excluded if the deformation parameter β_2 is large. Figure 2 shows the Coulomb dissociation cross sections calculated with $\beta_2 = 0.95$. The dashed and the solid lines correspond to the results in the adiabatic limit and those with the finite rotational energy, respectively. For this configuration, the cross sections show some jumps when a resonance state becomes a bound state as the separation energy increases so that its contribution is excluded in the sum in Eq. (12). In any case, the experimental cross sections can be reproduced when the separation energy is around 0.8 MeV, and thus this configuration cannot be excluded, although it is required that ^{31}Ne has a bound excited state

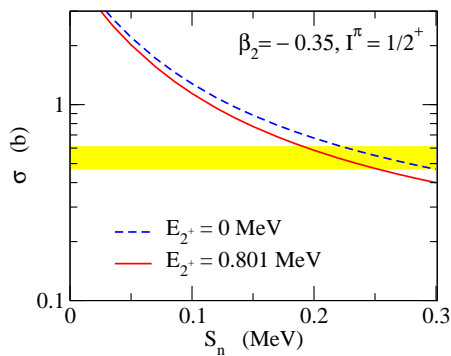


FIG. 3: (Color online) Same as Fig. 2, but for $\beta_2 = -0.35$. The corresponding Nilsson orbit is $[200\ 1/2]$ ($K^\pi = 1/2^+$), and the spin-parity of the ground state is $I^\pi = 1/2^+$.

and/or low-lying resonance states. For this configuration, the $[0^+ \otimes s_{1/2}]$ configuration is the main component of the wave function both in the adiabatic limit and in the non-adiabatic case (for instance, the probability is 80.5 % in the adiabatic limit and 79.2 % in the non-adiabatic case), and the non-adiabatic effect on the Coulomb dissociation is found to be small.

Although it may be unlikely that the ^{30}Ne nucleus is oblatelly deformed [23], the Coulomb dissociation data by themselves do not exclude a possibility of the oblate configuration corresponding to the $[200\ 1/2]$ ($K^\pi = 1/2^+$) Nilsson diagram at $\beta_2 \sim -0.35$. In order to demonstrate this, Fig. 3 shows the calculated Coulomb dissociation cross sections obtained with $\beta_2 = -0.35$. The spin-parity of the ground state is $I^\pi = 1/2^+$. As one can see, the experimental Coulomb dissociation cross sections can be well reproduced when $S_n \sim 0.2$ MeV. The main component of the wave function is the $[2^+ \otimes d_{3/2}]$ configuration

with an appreciable mixture of the $[0^+ \otimes s_{1/2}]$ configuration. The s -wave probability does not change much by the non-adiabatic effect, and the experimental data can be reproduced both in the adiabatic limit and in the non-adiabatic case.

In summary, we have discussed the E1 excitation of the ^{31}Ne nucleus using the particle-rotor model. The finite rotational excitation energy of the core nucleus has been taken into account. We have shown that the experimental cross sections can be well reproduced with the deformation parameter of $0.17 \lesssim \beta_2 \lesssim 0.33$ and the separation energy of $0.13 \lesssim S_n \lesssim 0.2$ MeV, for which the ground state configuration has the spin-parity of $I^\pi = 3/2^-$. However, the $I^\pi = 1/2^+$ configurations with large deformation around $\beta_2 \sim 0.95$ or with oblate deformation around $\beta_2 \sim -0.35$ cannot be excluded only from the Coulomb dissociation data. On the other hand, we have shown that the $I^\pi = 7/2^-$ configuration at $\beta_2 \sim 0.1$ and the $I^\pi = 3/2^-$ configuration at $\beta_2 \sim 0.55$ can be excluded due to the non-adiabatic effect, even though those configurations may reproduce the experimental data in the adiabatic limit.

For the ^{31}Ne nucleus, the momentum distribution for the nuclear breakup process [31] as well as the interaction cross section have been recently measured at the RIBF facility at RIKEN [32, 33]. It will be interesting to investigate whether our model can reproduce these experimental data simultaneously. We will report on it in a separate publication.

We thank T. Nakamura and K. Yoshida for useful discussions. This work was supported by the Grant-in-Aid for Scientific Research (C), Contract No. 22540262 and 20540277 from the Japan Society for the Promotion of Science.

-
- [1] I. Tanihata *et al.*, Phys. Rev. Lett. **55**, 2676(1985).
 - [2] I. Tanihata *et al.*, Phys. Lett. **B206**, 592 (1988).
 - [3] M. Fukuda *et al.*, Phys. Lett. **B268**, 339 (1991).
 - [4] T. Nakamura *et al.*, Phys. Rev. Lett. **83**, 1112 (1999).
 - [5] K. Riisager, A.S. Jensen, and P. Moller, Nucl. Phys. **A548**, 393 (1992).
 - [6] H. Sagawa, Phys. Lett. **B286**, 7 (1992).
 - [7] T. Nakamura *et al.*, Phys. Lett. **B394**, 11 (1997).
 - [8] T. Nakamura *et al.*, Phys. Rev. Lett. **96**, 252502 (2006).
 - [9] T. Nakamura *et al.*, Phys. Rev. Lett. **103**, 262501 (2009).
 - [10] T. Misu, W. Nazarewicz, and S. Aberg, Nucl. Phys. **A614**, 44 (1997).
 - [11] I. Hamamoto, Phys. Rev. C **69**, 041306(R) (2004).
 - [12] K. Yoshida and K. Hagino, Phys. Rev. C **72**, 064311 (2005).
 - [13] I. Hamamoto, Phys. Rev. C **81**, 021304(R) (2010).
 - [14] A. Poves and J. Retamosa, Nucl. Phys. **A571**, 221 (1994).
 - [15] P. Descouvemont, Nucl. Phys. **A655**, 440 (1999).
 - [16] P. Ring and P. Schuck, *The Nuclear Many Body Problem* (Springer-Verlag, New York, 1980).
 - [17] A. Bohr and B.R. Mottelson, *Nuclear Structure* (Benjamin, Reading, MA, 1975), Vol. II.
 - [18] D.M. Brink *et al.*, J. of Phys. **G13**, 629 (1987).
 - [19] H. Esbensen, B.A. Brown, and H. Sagawa, Phys. Rev. C **51**, 1274 (1995).
 - [20] F.M. Nunes, I.J. Thompson, and R.C. Johnson, Nucl. Phys. **A596**, 171 (1996).
 - [21] T. Tarutina and M.S. Hussein, Phys. Rev. C **70**, 034603 (2004).
 - [22] P. Doornenbal *et al.*, Phys. Rev. Lett. **103**, 032501 (2009).
 - [23] P. Fallon *et al.*, Phys. Rev. C **81**, 041302(R) (2010).
 - [24] B. Jurado *et al.*, Phys. Lett. **B649**, 43 (2007).
 - [25] S. Cwiok *et al.*, Comp. Phys. Comm. **46**, 379 (1987).
 - [26] H. Esbensen and C.N. Davids, Phys. Rev. C **63**, 014315 (2000).
 - [27] K. Hagino and N. Van Giai, Nucl. Phys. **A735**, 55 (2004).
 - [28] H. Esbensen and G.F. Bertsch, Nucl. Phys. **A542**, 310 (1992).
 - [29] C.A. Bertulani and G. Baur, Nucl. Phys. **A480**, 615 (1988).

- [30] A. Winther and K. Alder, Nucl. Phys. **A319**, 518 (1979).
- [31] W. Horiuchi *et al.*, Phys. Rev. **C81**, 024606 (2010).
- [32] T. Nakamura, private communication.
- [33] M. Takechi *et al.*, Nucl. Phys. **A834**, 412c (2010).